Reactive forcefield for simulating gold surfaces and nanoparticles

John A. Keith, Donato Fantauzzi, and Timo Jacob*
Institut für Elektrochemie, Universität Ulm, Albert-Einstein-Allee 47, D-89069 Ulm, Germany

Adri C. T. van Duin
Department of Mechanical and Nuclear Engineering, Pennsylvania State University, University Park, Pennsylvania 16801, USA
(Received 25 February 2010; revised manuscript received 6 May 2010; published 2 June 2010)

We present a ReaxFF reactive forcefield designed to reproduce first-principles density-functional theory (DFT) calculations on gold bulk structures, surfaces, and nanoparticles. We compare the ReaxFF results with those obtained from other atomistic potentials along with results from Perdew-Burke-Ernzerhof–generalized gradient approximation (PBE-GGA) DFT. The new ReaxFF gold force field, which has been trained against various bulk and surface properties calculated by DFT, is subsequently applied to simulated annealing simulations on a range of gold nanoparticles Au_n (n=38, 236, 1514).

DOI: 10.1103/PhysRevB.81.235404 PACS number(s): 82.20.Wt, 64.60.Cn, 31.15.es, 64.30.Ef

I. INTRODUCTION

Since the dawn of recorded history, gold has been one of the most desired metals on earth.[1] Its malleability and beauty have made it a common component in jewelry and currency, while its conductivity and resistance to oxidation have made it highly useful in modern-day applications in electronics, coatings, biotechnology, nanotechnology, and catalysis.

The past decades have seen tremendous growth in construction and characterization of thin films including self-assembled monolayers,[2–5] nanodevices,[6,7] and nanoparticles,[8–11] many of which involve gold explicitly. Gold's wide range of applications has stimulated many theoretical studies based on first-principles quantum mechanics (QM) calculations.[12–14] Despite modern advancements in computational technology, computational expense restricts QM studies to systems containing only a few hundred atoms, motivating many groups to develop parameters for empirical atomistic interaction potentials (so-called force fields) to rapidly simulate atomic-level phenomena on larger-scale systems.[15–33] Several significantly different classes of these potentials have already been compared by Grochola *et al.*[24]

In practice, empirical potentials are trained to reproduce useful physical data, however their parametrization sometimes limits their transferability to other applications. These potentials may provide bulk material properties or experimentally determined or first-principles calculated binding energies for molecular clusters. Their performance in applications outside of their parameterization scheme is not always well established, but an ideal interaction potential would be trusted for not only bulk systems, but for surfaces and clusters as well.

One robust approach, found in the embedded-atom method (EAM) (Refs. 15, 16, 21, and 22) as well as its modified form (MEAM),[23] is based on DFT and has been parameterized to efficiently reproduce experimental bulk material properties with relatively small computational expense. The main difference of the earlier EAM potential with the modified version is the latter's analytic expression for its embedding function, which includes angular forces coming from next-neighbor interactions. The (M)EAM approaches are very practical candidates for simulations of many-body effects of metallic systems, and they have been applied for a variety of general problems ranging from bulk properties to surfaces and even gaseous dimers.[34–36] However, since these methods are typically parameterized to reproduce bulk material properties, their utility may not be as robust in nonbulk simulations, i.e., surface reactions and for larger molecular clusters. Despite this, the efficiency of (M)EAM simulations make them attractive for some applications such as generating process barriers for kinetic Monte Carlo algorithms for surface reactions.

An alternative approach is to create interaction potentials based on first-principles calculations under a reactive force field scheme such as ReaxFF.[37] ReaxFF parameters are typically obtained by fitting analytic functions to DFT bonding curves. A recent study created a ReaxFF potential for gold.[33] This force field was fit entirely to DFT data calculated with the local spin density approximation (LSDA) exchange-correlation functional, a method generally considered appropriate for the morphology of bulk systems. The LSDA method is also usually used in obtaining necessary (M)EAM potentials for specific applications. It has been well established, however, that the LSDA treatment of electronic correlation, which is based on a homogeneous electron gas, makes LSDA methods less accurate for surface or cluster calculations.

The goal of the present work is to report how to construct ReaxFF potentials from first-principles data for broad material applications. Our new gold potential is capable of reproducing qualitative and quantitative features relating to binding energies and diffusion barrier profiles for surface processes, as well as bulk equations of state and effective cohesive energies of molecular clusters. The force field was parameterized entirely to DFT-data based on the generalized gradient approximation (GGA) exchange–correlation functional by Perdew-Burke-Ernzerhof (PBE)-GGA.[38] Inclusion of density gradients in GGA functionals make them more suitable for molecular structures and binding energies, though they are not usually better than LSDA calculations for bulk properties. An important goal for the present reactive forcefield is to allow studying nonidealized heterogeneous surface reactions and nanoparticles from first principles, so we believe this framework of QM is valuable and

can have many useful applications in heterogeneous catalysis and atomistic simulations of nanoscale systems.

II. METHODOLOGY

ReaxFF force fields have been a useful tool for atomistic simulations for nearly ten years.[37,39,40] Their form has been developed from principles established by the Tersoff[41] and Brenner[42] potentials. Unlike classical force fields designed for molecules such as UFF,[43,44] CHARMM,[45] OPLS,[46] or AMBER,[47,48] which require explicit bond definitions in molecular simulations, ReaxFF treats bonds implicitly, and its energy function is based on the concept of an atomic bond-order dependent on each atom's local environment. As such, reactive force fields are not constrained to common harmonic potentials and more realistic Lennard-Jones and Morse potential curves, which permit bond forming and breaking mechanisms, can be used. The dependence on bond order also means that most energy terms implicitly contain multibody contributions unlike many other atomistic potentials. For this study, the system energy for the gold force field contains three energy terms seen in Eq. (1).

$$E_{\text{system}} = E_{\text{bond}} + E_{\text{over}} + E_{\text{vdW}}, \tag{1}$$

where E_{bond} is the energy corresponding to interatomic bonds, E_{over} is a penalty energy that corrects atomic overcoordinations, and E_{vdW} accounts for van der Waals interactions and interatomic repulsions when atoms are too close to each other. The full expressions for these terms as well as the included parameters can be found in the Appendix.

We began training this force field by first computing the equations of state for several bulk structures of gold and included binding energies and self-diffusion processes on Au(100) surfaces. The purpose of investigating self-diffusion on Au(100) was to obtain a large database of diffusion processes under a wide range of defects that one might expect to exist on real surfaces. Besides simple terrace diffusion, we investigated diffusions along step edges, around inner- and outer-kink sites, and diffusions forming molecular dimers. Our DFT simulations on Au(100) surfaces utilized unit cells large enough to minimize unwanted lateral interactions, and details of these calculations can be found in previous work.[49,60]

We now will present our results from calculations with the new ReaxFF force field. In the following sections we compare our ReaxFF results to PBE-GGA values calculated with SEQQUEST (Ref. 50) as well as a selection of (M)EAM methods as calculated by LAMMPS,[51,52] an open source code that supports both ReaxFF and (M)EAM calculations. (M)EAM calculations include the original EAM method,[21,22] the original MEAM method (MEAM 1992),[23] and a revised MEAM method (MEAM 2003) (Ref. 35) that includes second nearest-neighbor interactions specifically fit to reproduce a different set of elastic constants.

III. RESULTS

A. Forcefield optimization

1. Bulk phases

The first stage of forcefield optimization involved parameterization of the fcc, bcc, ideal-hcp, sc, diamond, and a15 bulk phases of Au. The equations of state obtained from PBE-GGA (DFT) and our ReaxFF method are compared in Fig. 1. After optimization, this ReaxFF forcefield was capable of distinguishing several key features of the equations of states. For the fcc, bcc, hcp, and a15 structures, the ReaxFF well reproduces the binding energy, volume of minimum energy, and curvature of the binding well around the minimum compared to the PBE-GGA calculations used for parameterization. Based on the results summarized in Table I, noticeable differences are seen between calculated and experimental lattice constants, cohesive energies, and elastic constants. In general, (M)EAM methods do a rather impressive job of reproducing known experimental material properties, though one encounters small deviations between (M)EAM calculations for higher energy sc and diamond bulk phases. Only subtle differences are seen between calculated lattice constants (usually <0.1 Å), and reasonably small en-

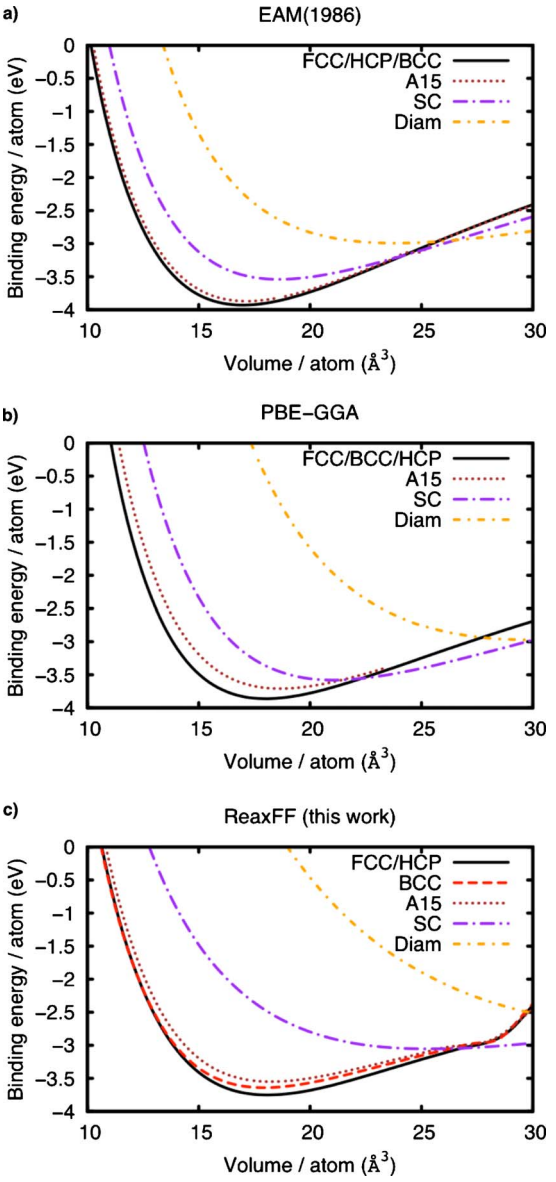

FIG. 1. (Color online) Equations of state for different Au bulk structures calculated by (a) EAM, (b) PBE-GGA, and (c) ReaxFF.

TABLE I. Calculated material constants for different phases of gold. Lattice constants (a_0) are reported in Å, cohesive energies (E_c) and cohesive energy differences with respect to the fcc structure (ΔE_c) are reported in eV, and bulk moduli (B) and elastic constants [$C_s=(C_{11}-C_{12})/2$ and C_{44}] are reported in GPa. Values marked with (*) denote elastic constants from a potential fit to a different set of data.

		ReaxFF	PBE-GGA	EAM (Ref. 21) (1986)	MEAM (Ref. 23) (1992)	MEAM (Ref. 35) (2003)	Expt.
fcc	a_0	4.18	4.16	4.08	4.07	4.08	4.08 (Ref. 53)
	E_c	3.77	3.85	3.93	3.93	3.93	3.93 (Ref. 54)
	B	143	158	167	167	179*	169 (Ref. 55)
	C_s	19	20	12	14.5	14*	12 (Ref. 55)
	C_{44}	55	53	45	42	41*	45 (Ref. 55)
bcc	a_0	3.31	3.32	3.24	3.14	3.18	
	E_c	3.63	3.83	3.91	3.91	3.92	
	B	150	148	166	160	182	
	ΔE_c	0.14	0.02	0.02	0.02	0.03	0.04 (Ref. 23)
a15	a_0	5.26	5.30	5.16	5.11	5.19	
	E_c	3.55	3.71	3.87	3.76	3.81	
	B	124	141	162	153	165	
	ΔE_c	0.22	0.14	0.06	0.17	0.14	
sc	a_0	2.95	2.75	2.65	2.62	2.65	
	E_c	3.08	3.60	3.54	3.81	3.73	
	B	36	56	123	126	151	
	ΔE_c	0.68	0.25	0.39	0.12	0.21	
diam	a_0	6.72	6.22	5.73	5.79	5.89	
	E_c	2.77	2.97	3.03	3.36	3.29	
	B	32	56	70	70	87	
	ΔE_c	1.00	0.88	0.91	0.58	0.66	

ergy differences are obtained (usually <0.1 eV) with the different (M)EAM methods, with the exception of high-energy sc and diamond phases. ReaxFF and PBE-GGA calculations, on the other hand, appear to generally overestimate lattice constants and underestimate binding energies compared to (M)EAM potentials and known experiment. Not surprisingly, calculated bulk moduli and elastic constants are generally not reproduced as well with (M)EAM methods.

Before discussing ReaxFF results specifically, one should note the apparent discrepancies between the phase diagrams calculated from EAM and PBE-GGA in Fig. 1. Since the semiempirical EAM method was parametrized to explicitly model bulk properties, we expect it to reasonably represent the different bulk structures of gold, and EAM results show an intersection of all six studied bulk structures at a volume of ~ 26 Å^3 while first-principles PBE-GGA does not. Certainly, LSDA may lead to more accurate QM-obtained equations of state as well as modern MEAM potentials.

In terms of reproducing PBE-GGA lattice constants, cohesive energies, bulk moduli, and elastic constants, ReaxFF performs respectably for the low-energy structures, but shows slightly larger deviations for the (less stable) high-energy structures. Indeed, during force field optimization less weight was given the reproduction of the high-energy (and therefore rather unlikely) sc and diamond structures. Nevertheless, ReaxFF curves are relatable to EAM and PBE-GGA equations of state. Perhaps most importantly, it is easily seen that the force field reproduces the qualitative preference of all bulk structures. If necessary, fundamental characteristics of these curves could always be improved to attain more accurate behavior, but in doing so one runs the risk of overparametrization. Since lower energy bulk structures are much more relevant in nature, the optimized force field turned out to even well reproduce PBE-GGA bulk elastic constants despite no attempts to specifically include these values in the ReaxFF training set. Finally, the discontinuities at atomic volumes >27 Å^3 are the result of the ReaxFF internal cutoff distance for bonds. However, these discontinuities are not crucial as the corresponding unit cell volumes already represent extremely harsh and most likely unphysical conditions.

2. *Surface calculations*

The second set of calculations focused on providing a training set for applicable surface calculations. Here we start with first comparing surface energies evaluated with ReaxFF to several other models (see Table II), including the previously used (M)EAM potentials, the so-called tight-binding linear muffin-tin orbital (TB-LMTO) method,[56] the full charge density (FCD)-LMTO method,[57] and the Green's function based full-potential screened Korringa-Kohn-Rostoker method (FP-KKR).[58] In general, all models reproduce similar trends of surface energies, though one can see

TABLE II. Calculated surface free energies for different (unreconstructed) low-index surfaces of gold. All energies are reported in J/m^2.

Au Surface	ReaxFF	EAM (Ref. 21) (1986)	MEAM (Ref. 23) (1992)	MEAM (Ref. 35) (2003)	TB-LMTO (Ref. 56) (1992)	FCD-LMTO (Ref. 57) (1998)	FP-KKR (Ref. 58) (2002)	Expt. (Ref. 59)
γ_{111}	1.76	0.79	0.89	0.93	1.61	1.28	1.39	1.5
γ_{100}	1.99	0.92	1.08	1.14	1.71	1.63	1.62	
γ_{110}	2.10	0.98	1.12	1.18	1.79	1.70	1.75	
$\Delta\gamma_{100-111}$	0.23	0.13	0.20	0.21	0.10	0.34	0.23	
$\Delta\gamma_{110-111}$	0.34	0.19	0.23	0.25	0.18	0.42	0.36	

some deficiencies with (M)EAM potentials here.

(M)EAM calculations underestimate surface free energies of gold, while the electronic structure calculations appear to capture the experimentally observed surface free energy reasonably well. Although no explicit information of surface energies entered our ReaxFF parametrization, we can already report surface energies in better agreement with experiment and other first-principles calculations than those reported from (M)EAM methods. ReaxFF appears to slightly overestimate surface energies, but the energy differences between different surfaces orientations fit almost exactly the FP-KKR calculations by Galanakis *et al.*[58] Regarding the well-known reconstructions of the low-index Au surfaces, we checked the missing-row reconstruction of Au(110). Here ReaxFF finds an extremely small preference for the unreconstructed surface (ca. 4×10^{-4} J/m^2), but this is well within the degree of precision one should expect from a semiempirical forcefield.

After the surface stabilities we focused on self-diffusion processes on Au(100). In previous extensive DFT studies, we simulated Au adatom binding and diffusion on the flat (terraced) surface, along and away from a step edge, in and out of kink sites of one or more rows of atoms thick, around and away from an outer kink site, into a step-edge defect, and different dissociations of an adsorbed Au dimer. Details of all processes can be found in Refs. 49 and 60. In Fig. 2 we report four notable examples.

Each of the four different diffusion profiles present a different challenge for an empirical potential. The first case [Fig. 2(a)], bridge diffusion on the Au(100) terrace, is the simplest diffusion profile for an adatom. In this case, our force field perfectly reproduces the PBE-GGA calculations, matching both its barrier height as well as its curvature across the barrier. The EAM method, however, provides a barrier ~0.1 eV lower than the PBE-GGA calculation and

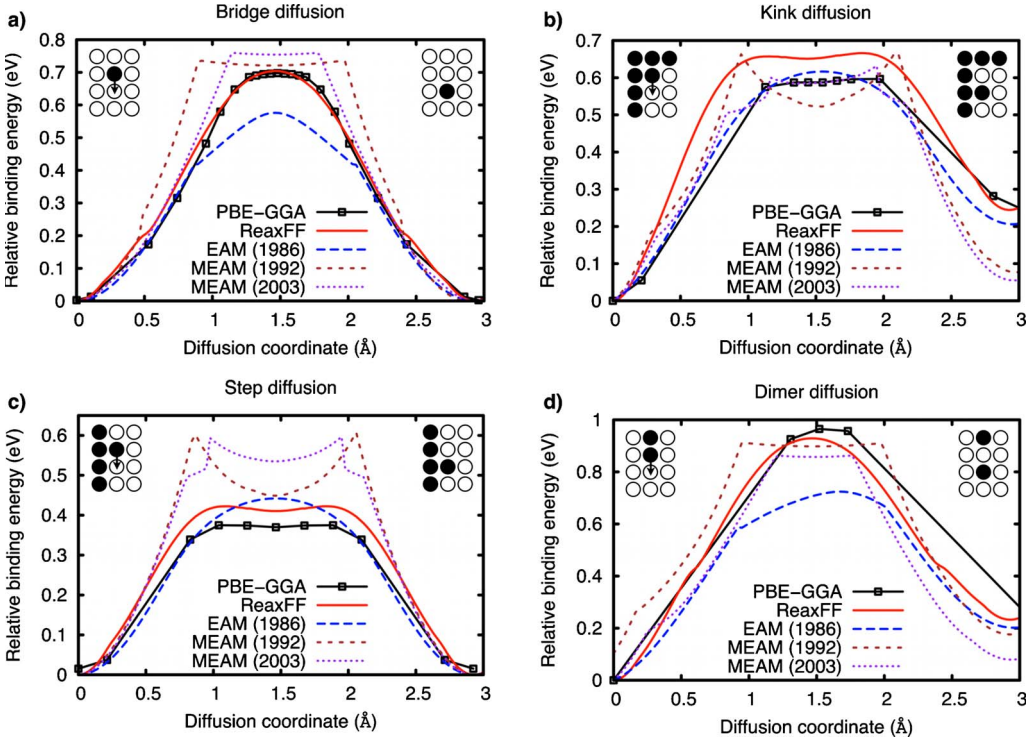

FIG. 2. (Color online) Selected Au diffusion pathways on an Au(100) surface. Insets in each figure illustrate the diffusion pathways, where open circles depict vacant sites and filled circles depict adatoms on an Au(100) surface. All diffusion pathways are described in detail in Refs. 49 and 60.

with a narrower peak at the summit of the barrier. These minor deviations should not be surprising since the EAM method was developed for bulk simulations. MEAM methods appear to correct the deficiencies in the classic EAM potential, though the shapes of the diffusion barriers are not continuous (most probably resulting from internal cutoffs) as one would expect in a self-diffusion process.

The second example, diffusion out of a kink site [Fig. 2(b)], has an adatom diffusing out of a site where it shares six nearest neighbors to a site where it shares five nearest neighbors. With the relatively high coordination of the diffusing adatom, this configuration of atoms is more comparable to a bulk structure than the rest. The calculated energy profiles of the (M)EAM potentials are in quite good agreement with DFT calculations, though only the MEAM(2003) potential captures both the correct curvature and the relative magnitude of the double well seen by PBE-GGA. Again, MEAM potentials display discontinuities in energies near the top of the barrier. In contrast, the ReaxFF calculated barrier is too high by a modest value of <0.1 eV, however, the double-well character found from DFT is still nicely reproduced. Interestingly, the relative energies of the intermediate states of both EAM and ReaxFF in the forward and reverse diffusion directions are both in excellent agreement with DFT calculations, but both MEAM potentials display some surface instability by showing the final structure of the diffusing atom to reside in a new state, ~ 0.15 eV lower in energy than the PBE-GGA value.

Figure 2(c) shows diffusion along a monoatomically high step edge. ReaxFF accurately reproduces the double-well diffusion character along a step edge, but the calculated barrier height is slightly higher (0.05 eV) than PBE-GGA. For the EAM simulation, the barrier is even a bit higher than ReaxFF, and does not qualitatively contain any double-well character observed from QM. Both MEAM potentials show double-well character, however the barriers are >0.2 eV too high, values more than $>50\%$ of the total process barrier.

The last example [Fig. 2(d)] considers dissociation of a dimer of adatoms on perfect Au(100). This example is also quite different from a bulk system, and it is not surprising that EAM underestimates the barrier obtained by DFT, as it did in the case of terrace diffusion. Likewise, MEAM potentials have higher and more accurate barriers than the EAM potential. The barrier calculated from our ReaxFF potential, however, is in very good agreement with DFT values. The MEAM(2003) potential again finds ~ 0.15 eV for the final structure after diffusion. Interestingly, in this particular case MEAM(1992) behaves differently. Similar to EAM and ReaxFF, MEAM(1992) leads to product states in excellent agreement with DFT values.

B. Applications to nanoparticles

After training the ReaxFF force field against bulk and surface diffusion properties, and describing that the optimized force field indeed is capable to reproduce the PBE-GGA calculated behavior, the remaining task is to test this force field against a set of data not being part of the optimization procedure. Therefore, in the following we will describe how the ReaxFF force field performs on the structure and stability of small Au clusters.

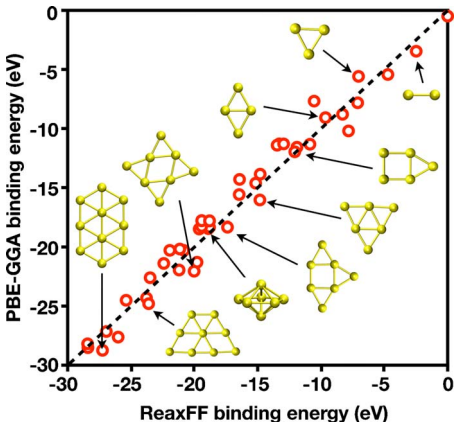

FIG. 3. (Color online) Comparison between PBE-GGA and ReaxFF calculated total binding energies for molecular gold clusters Au_n $(n=2-10)$. The models show the most stable structures obtained with DFT.

Many high quality studies have already reported QM structures for small neutral and anionic Au clusters, notably by (just to mention a few) Kappes,[61,62] Schwerdtfeger,[63,64] and Häkkinen.[13,65] These QM studies, however, aim on the most stable configurations and do not report the dynamical structures of nanoparticles and the degree that they might restructure under different environments.

In order to test the transferability of our own method, we calculated binding energies for several small gold clusters with both the final optimized ReaxFF force field and with DFT (again PBE-GGA) and compared those energies (see Fig. 3). For each cluster size we distinguished between various two- and three-dimensional configurations, which in case of DFT were additionally spin optimized.

We find that binding energies of neutral molecular clusters Au_n $(n=2-10)$ are reproduced quite well. As expected, total energies calculated by ReaxFF display slightly oscillatory behavior across different sizes and shapes of these clusters, but over the full range of 30 eV, these energies remain close to their PBE-GGA counterparts. Although the errors between ReaxFF and PBE-GGA are noticeable in Fig. 3, the error per atom for each cluster is <0.05 eV/atom with a standard deviation of 0.2 eV. That none of this data was incorporated into the ReaxFF training set is a testament to its capacity in more general simulations. Furthermore 2D structures, which are found as global minima in small clusters with high-level DFT,[13,61–65] are found as stable intermediates though not always as global minima. In comparison, EAM-like potentials find 2D structures are *unstable*.

Having established this ReaxFF as reliable for solids, surfaces, and clusters, we investigated the structural features of three arbitrarily sized gold nanoclusters. Our reactive molecular dynamics (MD) simulations focused on three clusters: Au_{38}, Au_{236}, and Au_{1514} under an imposed kinetic energy via a temperature thermostat (Berendsen thermostat). Spherical clusters were cut out from a bulk-fcc Au lattice. Each cluster was first equilibrated at 300 K for 12 ps using 0.25 fs time steps. The systems were then annealed at 1000,

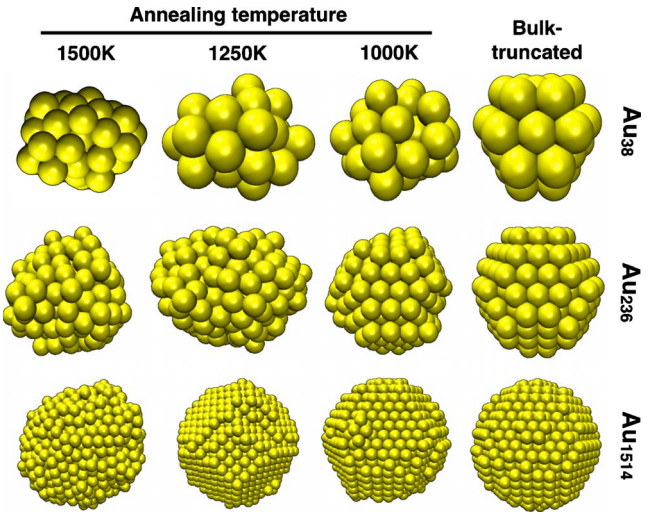

FIG. 4. (Color online) Gold clusters simulated with ReaxFF and their relaxed structures after different temperature annealing procedures.

1250, or 1500 K, heating with a temperature gradient of 0.05 K/step until the target temperature was reached for 300 000 iterations (75 ps simulation time). The clusters were then cooled at a slower rate, −0.01 K/step, until the system temperature reached 10 K. The high annealing temperatures are not used to explicitly reproduce material melting or sublimation of Au, but rather to give qualitatively different amounts of kinetic energy to the systems and see which structures become accessible when kinetic barriers to other structural phases are overcome. Figure 4 shows both the initial bulk-truncated clusters as well as the final relaxed structures from these simulations.

In studies on the Au_{38} cluster, annealing led to amorphous structures at 1000, 1250, and 1500 K. The same transition to an amorphous cluster was observed for the Au_{236} cluster when heating to 1250 and 1500 K. When annealing at 1000 K, however, the supported kinetic energy is too low to allow for substantial morphology changes compared to the initial bulk-truncated structure. The minimum annealing temperature for structure changes is even higher for Au_{1514}, which remains largely unperturbed until it is annealed to 1500 K, where it too becomes amorphous. Based on these results, one sees a clear trend showing a direct relationship between nanoparticle size and the barrier to form an amorphous material.

To better analyze the mechanism for how these nanoparticles transform into amorphous clusters, we investigated the coordination numbers of all atoms of different annealed structures in the Au_{1514} cluster (see Fig. 5). In the temperature range where the bulk (i.e., subsurface) structure is maintained (0–1250 K), the largest percentage of atoms have coordination numbers of 12, showing that they are atoms within a bulk-fcc lattice. As annealing temperatures increase, one sees that the final relaxed structures show a small spike in numbers of atoms having coordination numbers of 9. This corresponds to an increase in atoms on a Au(111) surface. When this cluster is annealed at 1500 K, a phase transition takes place, and the gold nanoparticle becomes amorphous as clearly seen in Fig. 6.

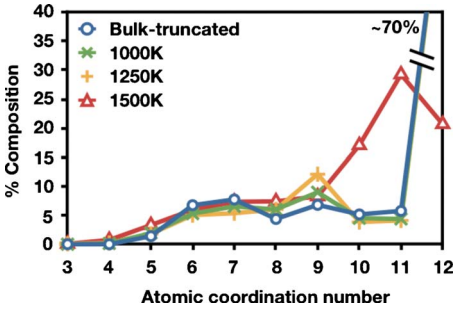

FIG. 5. (Color online) The percent composition of gold atoms with different coordination numbers. The different curves are for the initial bulk-truncated Au_{1514} cluster and after annealing at 1000, 1250, and 1500 K.

Within this framework, additional morphology studies on other nanoparticles, such as the prominent Au_{55} cluster are possible. We have already run dynamics simulations on >3000 different Au_{55} structures to find its lowest-energy geometry. Although a wide range of structures are found very close in energy, we found the icosohedral structure to be most stable. More thorough investigations on gold nanoparticles will be the aim of future work.

IV. CONCLUSIONS

We have developed a new Au potential within the framework of the ReaxFF class of reactive force fields. This potential has been based on first-principles PBE-GGA data, and is capable of reproducing important features of the Au bulk equations of state. This potential also shows quite good agreement with the first-principles data for surface diffusion reactions, and sometimes displays noticeable differences with surface calculations with other gold potentials in the family of (M)EAM methods. Furthermore, without explicit parameterization, this variant of ReaxFF is capable of capturing the stabilities of Au single crystal surfaces as well as

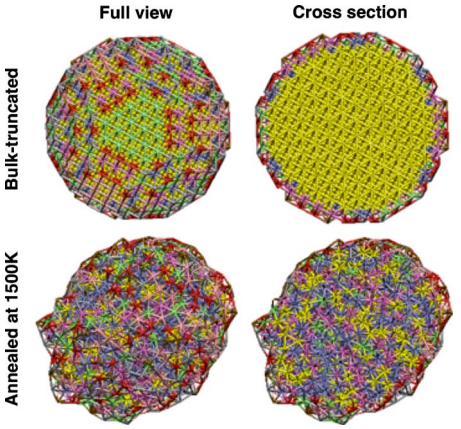

FIG. 6. (Color online) Illustrations of the Au_{1514} cluster before and after annealing at 1500 K. Atoms are colored according to their coordination numbers. Models on the left show the outer shell of the full nanoparticle, while models on the right show the nanoparticles with cross-sectional cut to show their cores.

binding energies of small nanoclusters of gold.

This ReaxFF potential has been applied to study the structure of nanoparticles of different sizes under different temperature regimes to access the morphology of new nanoparticle structures. We find that over the course of an annealing procedure, well-ordered structures become amorphous at high temperature, and large nanoparticles annealed at high temperatures can then relax into a differently structured nanoparticle when cooled. That such phase transitions occur may potentially affect how nanoparticles are viewed under ambient reaction conditions and how their catalytic properties can be interpreted.

The aim of the present work was to present and test our new ReaxFF force field for Au bulk, surfaces, and nanoparticles. In later work, we aim to apply this force field to provide in-depth analysis of accessible structures for a wide distribution of Au nanoparticles.

ACKNOWLEDGMENTS

Support from the Alexander von Humboldt Foundation (AvH), the Fonds der Chemischen Industrie (FCI), and the Deutsche Forschungsgemeinschaft (DFG) within the Emmy-Noether Program are gratefully acknowledged. A.C.T.v.D. acknowledges support from the startup Grant No. KISK C000032472.

APPENDIX: REAXFF FUNCTIONS AND PARAMETERS

In the ReaxFF formalism, the functional form of the energy terms in Eq. (1) are the following. Optimized values for the parameters herein are found in Table III. The bond energy term,

$$E_{\text{bond}} = -D_e^{\sigma} BO_{ij}^{\sigma} \exp\{p_{\text{be1}}[1-(BO_{ij}^{\sigma})^{p_{\text{be2}}}]\}, \tag{A1}$$

where, BO_{ij}^{σ}, the bond order of the σ-bond between atoms i and j is

$$BO_{ij}^{\sigma} = \exp\left[p_{\text{bo1}}\left(\frac{r_{ij}}{r_0^{\sigma}}\right)^{p_{\text{bo2}}}\right]. \tag{A2}$$

The van der Waals energy term, which includes repulsive energies when atoms are too close together, is

TABLE III. Optimized parameters of the ReaxFF potential for gold.

General Parameters	p_{vdW1}	1.5591
Atom parameters	r_0^{σ} (Å)	2.0074
	$p_{\text{ovun 2}}$	−24.8303
	Val	1.0000
vdW parameters	r_{vdW} (Å)	2.1413
	D_{vdW}(kcal mol^{-1})	0.3730
	α_{vdW}	12.1061
	γ_{vdW}(Å^{-1})	2.1635
Bond parameters	D_e^{σ}(kcal mol^{-1})	142.6814
	p_{bo1}	−0.1517
	p_{bo2}	5.2066
	p_{be1}	−0.0100
	p_{be2}	0.2903
	p_{ovun1}	0.3663

$$E_{\text{vdW}} = T(r_{ij}) D_{\text{vdW}} \left\{ \exp\left[\alpha_{ij}\left(1-\frac{f_{13}(r_{ij})}{r_{\text{vdW}}}\right)\right] - 2\exp\left[\frac{1}{2}\alpha_{ij}\left(1-\frac{f_{13}(r_{ij})}{r_{\text{vdW}}}\right)\right]\right\} \tag{A3}$$

where the Taper correction:

$$T(r) = \frac{20}{R_{\text{cut}}^7} r^7 - \frac{70}{R_{\text{cut}}^6} r^6 + \frac{49}{R_{\text{cut}}^5} r^5 + 1, \tag{A4}$$

uses the arbitrary cutoff of $R_{\text{cut}}=10$ Å, and

$$f_{13}(r_{ij}) = [(r_{ij})^{p_{\text{vdW1}}} + (\gamma_{\text{vdW}})^{-p_{\text{vdW1}}}]^{1/p_{\text{vdW1}}}. \tag{A5}$$

The energy contribution of overcoordinated atoms is

$$E_{\text{over}} = \frac{\sum_{j=1}^{n} (p_{\text{ovun1}} D_e^{\sigma} BO_{ij}^{\sigma})}{\Delta + \text{Val}} \frac{\Delta}{[1+\exp(p_{\text{ovun2}}\Delta)]}, \tag{A6}$$

where Δ is difference between ideal and actual coordination of each atom:

$$\Delta = -\text{Val} + \sum_{j=1}^{n} BO_{ij}^{\sigma}, \tag{A7}$$

and n is the number of bonds associated with atom i due to atom(s) j.

*timo.jacob@uni-ulm.de; http://www.echem.uni-ulm.de

[1] For more information see http://www.gold.org
[2] S. Lim and C. Zhong, Acc. Chem. Res. **42**, 798 (2009).
[3] D. Zacher, O. Shekhah, C. Wöll, and R. A. Fischer, Chem. Soc. Rev. **38**, 1418 (2009).
[4] G. Zotti, B. Vercelli, and A. Berlin, Acc. Chem. Res. **41**, 1098 (2008).
[5] J. Love, L. Estroff, J. Kriebel, R. Nuzzo, and G. Whitesides, Chem. Rev. (Washington, D.C.) **105**, 1103 (2005).
[6] M. Pollard, M. ter Wiel, R. van Delden, J. Vicario, N. Koumura, C. van den Brom, A. Meetsma, and B. Feringa, Chem.-Eur. J. **14**, 11610 (2008).
[7] H. Nishihara, K. Kanaizuka, Y. Nishimori, and Y. Yamanoi, Coord. Chem. Rev. **251**, 2674 (2007).
[8] M. Cortie and A. McDonagh, in *Gold Chemistry*, edited by F. Mohr (Wiley-VCH Verlag GmbH & Co, Weinheim, Germany,

2009), pp. 321–356.
[9] D. Graham, K. Faulds, D. Thompson, F. McKenzie, R. Stokes, C. Dalton, R. Stevenson, J. Alexander, P. Garside, and E. McFarlane, Biochem. Soc. Trans. **37**, 697 (2009).
[10] R. Sardar, A. M. Funston, P. Mulvaney, and R. W. Murray, Langmuir **25**, 13840 (2009).
[11] D. Vanmaekelbergh, Nat. Nanotechnol. **4**, 475 (2009).
[12] P. Pyykkö, Chem. Soc. Rev. **37**, 1967 (2008).
[13] H. Häkkinen, Chem. Soc. Rev. **37**, 1847 (2008).
[14] S. Venkatachalam, P. Kaghazchi, L. A. Kibler, D. M. Kolb, and T. Jacob, Chem. Phys. Lett. **455**, 47 (2008).
[15] M. S. Daw and M. I. Baskes, Phys. Rev. Lett. **50**, 1285 (1983).
[16] M. S. Daw and M. I. Baskes, Phys. Rev. B **29**, 6443 (1984).
[17] J. Cai and Y. Y. Ye, Phys. Rev. B **54**, 8398 (1996).
[18] H. Chamati and N. Papanicolaou, J. Phys.: Condens. Matter **16**, 8399 (2004).
[19] F. Cleri and V. Rosato, Phys. Rev. B **48**, 22 (1993).
[20] F. Ercolessi, M. Parrinello, and E. Tosatti, Philos. Mag. A **58**, 213 (1988).
[21] S. M. Foiles, M. I. Baskes, and M. S. Daw, Phys. Rev. B **33**, 7983 (1986).
[22] S. M. Foiles, M. I. Baskes, and M. S. Daw, Phys. Rev. B **37**, 10378 (1988).
[23] M. I. Baskes, Phys. Rev. B **46**, 2727 (1992).
[24] G. Grochola, S. P. Russo, and I. K. Snook, J. Chem. Phys. **123**, 204719 (2005).
[25] G. C. Kallinteris, N. I. Papanicolaou, G. A. Evangelakis, and D. A. Papaconstantopoulos, Phys. Rev. B **55**, 2150 (1997).
[26] T. J. Raeker and A. E. Depristo, Int. Rev. Phys. Chem. **10**, 1 (1991).
[27] S. B. Sinnott, M. S. Stave, T. J. Raeker, and A. E. DePristo, Phys. Rev. B **44**, 8927 (1991).
[28] M. S. Stave, D. E. Sanders, T. J. Raeker, and A. E. DePristo, J. Chem. Phys. **93**, 4413 (1990).
[29] A. Voter, Los Alamos Unclassified Technical Report No. LA-UR-93–3901, 1993 (unpublished).
[30] X. D. Dai, Y. Kong, and J. H. Li, Phys. Rev. B **75**, 104101 (2007).
[31] S. Olivier, R. Conte, and A. Fortunelli, Phys. Rev. B **77**, 054104 (2008).
[32] N. Wilson and R. Johnston, Eur. Phys. J. D **12**, 161 (2000).
[33] T. Järvi, A. Kuronen, M. Hakala, K. Nordlund, A. C. T. van Duin, W. A. Goddard III, and T. Jacob, Eur. Phys. J. B **66**, 75 (2008).
[34] M. I. Baskes, Phys. Rev. Lett. **83**, 2592 (1999).
[35] B.-J. Lee, J.-H. Shim, and M. I. Baskes, Phys. Rev. B **68**, 144112 (2003).
[36] C. L. Kuo and P. Clancy, Modell. Simul. Mater. Sci. Eng. **13**, 1309 (2005).
[37] A. C. T. van Duin, S. Dasgupta, F. Lorant, and W. A. Goddard, J. Phys. Chem. A **105**, 9396 (2001).
[38] J. P. Perdew, K. Burke, and M. Ernzerhof, Phys. Rev. Lett. **77**, 3865 (1996).
[39] A. van Duin, in *Computational Methods in Catalysis and Materials Science*, edited by R. van Santen and P. Sautet (Wiley-VCH Verlag GmbH & Co., Weinheim, Germany, 2009), pp. 167–181.
[40] K. D. Nielson, A. C. T. van Duin, J. Oxgaard, W. Deng, and W. A. Goddard, J. Phys. Chem. A **109**, 493 (2005).
[41] J. Tersoff, Phys. Rev. B **39**, 5566 (1989).
[42] D. W. Brenner, Phys. Rev. B **42**, 9458 (1990).
[43] C. J. Casewit, K. S. Colwell, and A. K. Rappe, J. Am. Chem. Soc. **114**, 10046 (1992).
[44] A. K. Rappe, C. J. Casewit, K. S. Colwell, W. A. Goddard, and W. M. Skiff, J. Am. Chem. Soc. **114**, 10024 (1992).
[45] B. R. Brooks, R. E. Bruccoleri, B. D. Olafson, D. J. States, S. Swaminathan, and M. Karplus, J. Comput. Chem. **4**, 187 (1983).
[46] W. Damm, A. Frontera, J. Tirado-Rives, and W. L. Jorgensen, J. Comput. Chem. **18**, 1955 (1997).
[47] W. D. Cornell, P. Cieplak, C. I. Bayly, I. R. Gould, K. M. Merz, D. M. Ferguson, D. C. Spellmeyer, T. Fox, J. W. Caldwell, and P. A. Kollman, J. Am. Chem. Soc. **117**, 5179 (1995).
[48] W. D. Cornell, P. Cieplak, C. I. Bayly, I. R. Gould, K. M. Merz, D. M. Ferguson, D. C. Spellmeyer, T. Fox, J. W. Caldwell, and P. A. Kollman, J. Am. Chem. Soc. **118**, 2309 (1996).
[49] K. Pötting, W. Schmickler, and T. Jacob, in *High Performance Computing in Science and Engineering '06*, edited by W. Nagel, W. Jäger, and M. Resch (Springer-Verlag GmBH, Heidelberg, Germany, 2007), pp. 171–185.
[50] C. Verdozzi, P. A. Schultz, R. Wu, A. H. Edwards, and N. Kioussis, Phys. Rev. B **66**, 125408 (2002).
[51] S. J. Plimpton, J. Comput. Phys. **117**, 1 (1995).
[52] LAMMPS website: http://lammps.sandia.gov
[53] N. W. Ashcroft and N. D. Mermin, *Solid State Physics* (Holt, Reinhart and Winston, New York, 1976).
[54] C. J. Smith, *Metal Reference Book* (Butterworths, London, 1976), p. 186.
[55] G. Simmons and H. Wang, *Single Crystal Elastic Constants and Calculated Aggregate Properties: A Handbook*, 2nd ed. (MIT Press, Cambridge, MA, 1971).
[56] H. L. Skriver and N. M. Rosengaard, Phys. Rev. B **46**, 7157 (1992).
[57] L. Vitos, A. V. Ruban, H. L. Skriver, and J. Kollár, Surf. Sci. **411**, 186 (1998).
[58] I. Galanakis, N. Papanikolaou, and P. H. Dederichs, Surf. Sci. **511**, 1 (2002).
[59] W. Tyson and W. A. Miller, Surf. Sci. **62**, 267 (1977).
[60] K. Pötting, W. Schmickler, and T. Jacob, ChemPhysChem **11**, 1395 (2010).
[61] M. P. Johansson, A. Lechtken, D. Schooss, M. M. Kappes, and F. Furche, Phys. Rev. A **77**, 053202 (2008).
[62] A. Lechtken, D. Schooss, J. Stairs, M. Blom, F. Furche, N. Morgner, and O. Kostko, B. von Issendorff, and M. Kappes, Angew. Chem., Int. Ed. **46**, 2944 (2007).
[63] B. Assadollahzadeh and P. Schwerdtfeger, J. Chem. Phys. **131**, 064306 (2009).
[64] P. Schwerdtfeger, Angew. Chem., Int. Ed. **42**, 1892 (2003).
[65] H. Häkkinen and U. Landman, Phys. Rev. B **62**, R2287 (2000).